

HENRY

Hydraulic Engineering Repository

Ein Service der Bundesanstalt für Wasserbau

Article, Published Version

Holzwarth, Ingrid; Weilbeer, Holger; Wirtz, Kai W.

The effect of bathymetric modification on water age in the Elbe Estuary

Die Küste

Zur Verfügung gestellt in Kooperation mit/Provided in Cooperation with:
Kuratorium für Forschung im Küsteningenieurwesen (KFKI) (Hg.)

Verfügbar unter/Available at: <https://hdl.handle.net/20.500.11970/107397>

Vorgeschlagene Zitierweise/Suggested citation:

Holzwarth, Ingrid; Weilbeer, Holger; Wirtz, Kai W. (2019): The effect of bathymetric modification on water age in the Elbe Estuary. In: Die Küste 87. Karlsruhe: Bundesanstalt für Wasserbau. S. 261-282. <https://doi.org/10.18171/1.087109>.

Standardnutzungsbedingungen/Terms of Use:

Die Dokumente in HENRY stehen unter der Creative Commons Lizenz CC BY 4.0, sofern keine abweichenden Nutzungsbedingungen getroffen wurden. Damit ist sowohl die kommerzielle Nutzung als auch das Teilen, die Weiterbearbeitung und Speicherung erlaubt. Das Verwenden und das Bearbeiten stehen unter der Bedingung der Namensnennung. Im Einzelfall kann eine restriktivere Lizenz gelten; dann gelten abweichend von den obigen Nutzungsbedingungen die in der dort genannten Lizenz gewährten Nutzungsrechte.

Documents in HENRY are made available under the Creative Commons License CC BY 4.0, if no other license is applicable. Under CC BY 4.0 commercial use and sharing, remixing, transforming, and building upon the material of the work is permitted. In some cases a different, more restrictive license may apply; if applicable the terms of the restrictive license will be binding.



The effect of bathymetric modification on water age in the Elbe Estuary

Ingrid Holzwarth¹, Holger Weilbeer¹ and Kai W. Wirtz²

¹ Bundesanstalt für Wasserbau

² Helmholtz-Zentrum Geesthacht

Summary

The transport time of substances is a physical factor that influences the completeness of biogeochemical reactions in the estuary. Since hydrodynamic changes induce changes in transport time, river discharge and its seasonal variability strongly determine the transport time of riverine water and its fluctuations.

A factor that leads to a permanent change in hydrodynamics is man-made bathymetric modification. However, the impact of such modification on transport time has never been quantified. Here we show for the Elbe Estuary (Germany), an example of a partially to well-mixed alluvial estuary, that the impact of typical, decadal man-made bathymetric modification on the transport time of riverine water is much smaller than the effect of the natural variability in river discharge. In this study, we used riverine water age to determine transport time. We found the age difference due to river discharge variation to be in the order of days to weeks, depending on the location within the estuary. In contrast to the strong influence of discharge, we found the age difference between scenarios which differ by the effect of 40 years of man-made bathymetric modification to be in the order of hours with a maximum of 38 hours, depending on location and discharge. Overall, riverine water age increases by approximately 7 % in the more strongly impacted bathymetry, suggesting that transport time is only slightly affected by the considerable depth differences of several meters in large parts of the estuary.

With regard to the summer oxygen minimum zone, which regularly develops in the estuarine freshwater section, we therefore expect the physical influence of the realistic modification via a change in transport time to be small. Nevertheless, the increase in transport time of land-borne material potentially poses an additional stressor to the dissolved oxygen dynamics in the estuary.

Keywords

well-mixed estuary; bathymetric modification; transport time; riverine water age; hydraulic residence time

Zusammenfassung

Die Dauer des Stofftransportes entlang eines Ästuars ist ein physikalischer Faktor, der die Vollständigkeit der stattfindenden biogeochemischen Umsetzungen beeinflusst. Die Transportzeit des Wassers und der sich darin befindenden gelösten und suspendierten Stoffe wird durch die Hydrodynamik bestimmt, sodass

Änderungen in der Hydrodynamik auch Änderungen in der Transportzeit hervorrufen; die Transportzeit des flussseitig in das Ästuar einströmenden Wassers ist besonders von dessen Menge und deren Variabilität abhängig.

Bathymetrische Anpassungen rufen eine dauerhafte Änderung der Hydrodynamik hervor. Dennoch wurde bisher der Einfluss von menschengemachten Anpassungen der Ästuarbathymetrie auf die Transportzeit nicht quantifiziert. Für das Ästuar der Elbe (Deutschland), als ein Beispiel eines teilweise bis gut durchmischten alluvialen Ästuars, zeigen wir, dass der Einfluss typischer menschengemachter Anpassungen der Bathymetrie auf die Transportzeit kleiner ist als der Einfluss der natürlichen Variabilität des Oberwasserzuflusses.

Dazu bestimmten wir das Wasseralter des Oberwassers im Ästuar und fanden die Unterschiede im Wasseralter aufgrund der Variabilität der Oberwassermenge in der Größenordnung von Tagen bis Wochen, abhängig von der Position im Ästuar. Im Unterschied zu dem starken Einfluss der Oberwassermenge zeigte sich der Unterschied im Wasseralter zwischen zwei bathymetrischen Szenarien, die sich durch den Effekt von 40 Jahren menschlicher Einflüsse auf die Bathymetrie unterschieden, in der Größenordnung von Stunden bis hin zu einem Tag. Insgesamt betrug die Zunahme des Wasseralters etwa 7 % in dem Szenario mit der menschlich stärker beeinflussten Bathymetrie und den teilweise großen Tiefenänderungen von mehreren Metern.

Im Hinblick auf die Zone des sommerlichen Sauerstoffminimums, die sich regelmäßig im Süßwasserteil des Elbeästuars entwickelt, ist daher der rein physikalische Einfluss der bathymetrischen Änderungen durch die Transportzeit als klein zu erwarten. Dennoch stellt auch die geringe Erhöhung der Transportzeit potentiell einen zusätzlichen Stressor für die Sauerstoffdynamik des Ästuars dar.

Schlagwörter

gut durchmischtes Ästuar; bathymetrische Anpassungen; Transportzeit; Wasseralter; Aufenthaltszeit

1 Introduction

The transport time of land-borne substances in estuaries is an important characteristic because it is the physical factor that influences the completeness of biogeochemical reactions in the estuary or certain estuarine sections. In the context of nutrient transport, phytoplankton dynamics, low oxygen situations, fate of pollutants and spill events, such transport times have been assessed in many estuarine systems worldwide (Ahmed et al. 2017, Brye et al. 2012, Chan et al. 2002, Fujiwara et al. 2002, Rayson et al. 2016, Shen and Haas 2004). Usually, a strong dependence of transport time on river discharge is either inherently given by the applied method, e.g. in (Sheldon and Alber 2006), or observed in the results, e.g. in (Kärnä and Baptista 2016).

Generally, changes in transport time are induced by changes in hydrodynamics. Thus, several other influence mechanisms than river discharge on transport time scales exist; of particular interest are man-made influences with regard to the interaction of the diverse impacts on the biogeochemical system of estuaries. One of the man-made interventions to which many estuaries worldwide are subjected to nowadays, is the deepening of the estuarine bathymetry for navigational purpose (Abood et al. 1999, Avoine et al. 1981, Meyers et al. 2014, van Maren et al. 2015, Vriend et al. 2011). While bathymetric changes involve changes in estuarine hydrodynamics (Ensing et al. 2015, Lane 2004, Liu et al. 2001, Picado et al. 2010, Prandle 2003) they potentially also induce a change in transport time. Despite

the ubiquity of bathymetric deepening, the influence of man-made bathymetric modification on transport time has not been quantitatively investigated to date.

Several methods exist to estimate time scales for the transport of substances. Some methods provide an integral time scale for the entire system; others give local results for the different positions in the estuary (Zimmerman 1988). The former kind of methods are so-called box model estimates (Kärnä and Baptista 2016, Zimmerman 1988) which usually either base on the flushing time approach (Monsen et al. 2002, Zimmerman 1988), make use of particle tracking methods (Rayson et al. 2016) or rely on tidal prism models (Luketina 1998). Local time scales are either section-wise applications of the box model estimates, or continuous methods that make use of numerical models. Of those local and continuous methods, the concept of water age is a widely used method (Brye et al. 2012, Kärnä and Baptista 2016, Shen and Haas 2004); it is mathematically well-described (Deleersnijder et al. 2001, Delhez et al. 1999, Delhez et al. 2004, Delhez et al. 2014, Delhez and Deleersnijder 2002) and demarcated from related time scales (Delhez et al. 2014).

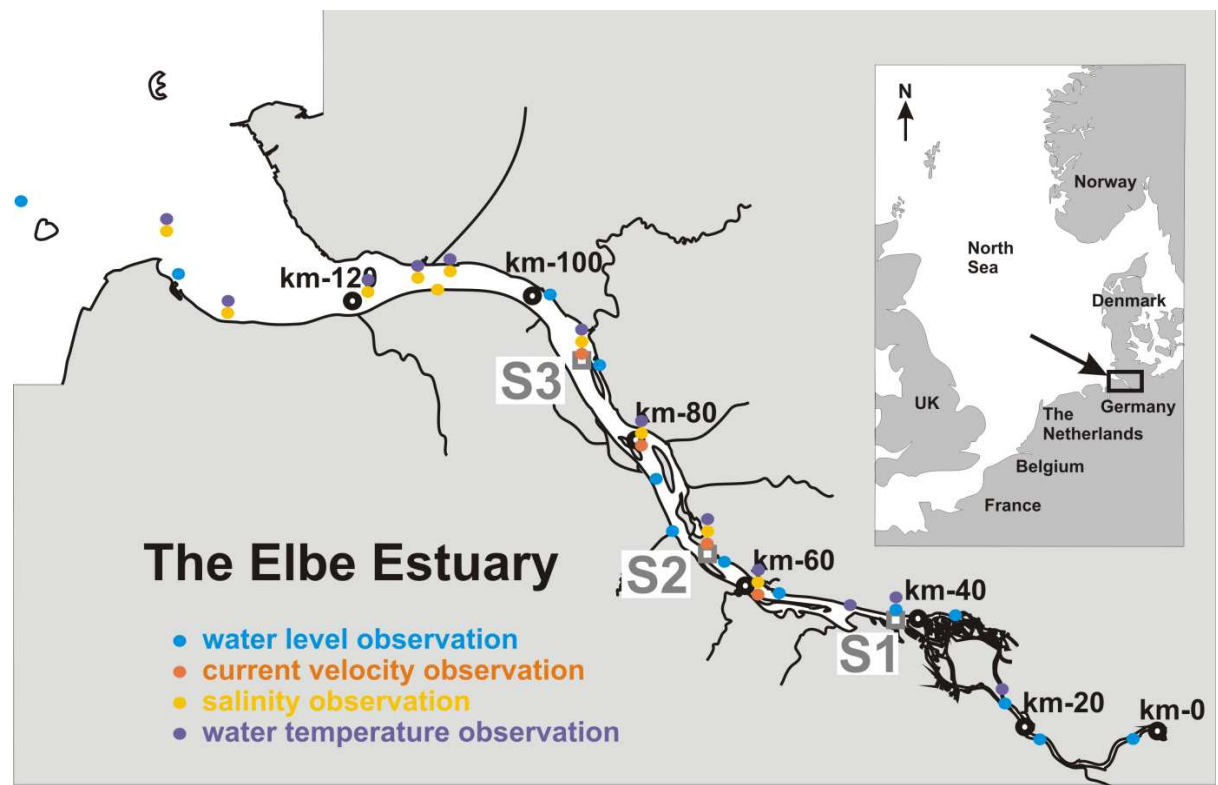


Figure 1: Location of the Elbe Estuary at the North Sea (small map). Thick black circles mark the distance in kilometers downstream of the tidal barrier at km-0. The blue circles show the position of the gauges (from upstream to downstream) Altengamme, Over, Bunthaus, Hamburg St. Pauli, Seemannshoef, Schulau, Hetlingen, Stadersand, Grauerort, Glueckstadt, Brokdorf, Cuxhaven, and Scharhoern. The most downstream gauging station Bake Alpha lies outside of the map. The orange circles show the position of the observation stations for current velocity (from upstream to downstream) D1 Hanskalbsand, D2 Julesand, D3 Pagensand, D4 Rhinplate. The yellow circles show the position of the salinity observation stations (from upstream to downstream) D1 Hanskalbsand, D2 Julesand, D3 Pagensand, D4 Rhinplate, LZ1a, LZ1, LZ1b, LZ2, LZ3 and LZ4. The violet circles show the position of the water temperature observation stations (from upstream to downstream) Bunthaus, Seemannshoef, Blankenese, D1 Hanskalbsand, D2 Julesand, D3 Pagensand, D4 Rhinplate, LZ1a, LZ1b, LZ2, LZ3 and LZ4. The three grey squares mark the specific positions S1, S2 and S3 for the analysis later on.

In this study, we examine the effect of a realistic bathymetric change on transport time scale. The bathymetric change reflects 40 years of human interference in the Elbe Estuary (Germany), see Figure 1. According to the classification of Savenije (2005), the Elbe Estuary is a funnel shaped alluvial estuary with an amplification of the tide in upstream direction. In the estuarine parameter space of Geyer and MacCready (2014), the Elbe Estuary extends from well-mixed to partially mixed conditions, depending on the position within the estuary. The Elbe Estuary is strongly exposed to anthropogenic influences, particularly by strong man-made modifications of its geometry with considerable deepening of the bathymetry during the last centuries, but also by riverine substance loads which lead to strong biogeochemical processes and the formation of a seasonal oxygen minimum zone in the estuarine freshwater section (Amann et al. 2012, 2014, Bergemann et al. 1996, Dähnke et al. 2008, Schöl et al. 2014, Schroeder 1997).

2 Method

2.1 Hydrodynamic model

We simulated hydrodynamics in the Elbe Estuary with the mathematical method Untrim (Casulli 2009, Casulli and Stelling 2010). The Elbe Estuary model setup is adapted from the coarsest model described in (Sehili et al. 2014). In comparison to the model used there, the largest difference in the model applied here is the use of a detailed distribution of bottom friction coefficients. The bathymetry resolution on subgrid level (Casulli and Stelling 2010) enables a precise representation of water volume. The unstructured, orthogonal computational grid consists of roughly 11000 horizontal elements with 25 subgrid divisions per edge and a maximum of 31 vertical z-layers with a thickness of 1m.

The model domain extends along the 170 km estuarine shipping channel, starting at the weir Geesthacht (km-0, see Figure 1) down to the end of the maintained shipping channel in the inner German Bight, see Figure 2a. The domain contains the entire volume between the main dikes and includes the largest eight tributaries of the estuary.

The model is steered with realistic boundary values for the years 2010 and 2011: at the riverine boundary, we use daily measurements of river discharge at the last riverine gauging station Neu Darchau (50 km upstream of the weir at km-0; data from Water and Shipping Authority Lauenburg, accessed at www.fgg-elbe.de). The highest discharge during the simulation period occurred at the end of January 2011 with a peak value of $3500 \text{ m}^3 \text{ s}^{-1}$, and long-lasting low discharge, ranging between $300\text{--}500 \text{ m}^3 \text{ s}^{-1}$, was observed from May to end of July 2011. Riverine water temperatures have a clear seasonal cycle with lowest values of $2\text{--}5^\circ\text{C}$ at the beginning of the year, and highest values of $20\text{--}23^\circ\text{C}$ during June to September. Riverine water temperatures originate from observations at the station Cumlosen (115 km upstream of the weir at km-0; data from Landesamt für Umwelt Brandenburg, accessed at www.fgg-elbe.de).

The boundary value for salinity is kept constant at 0.4 psu. In the tributaries we employ long-term mean discharge estimates (IKSE 2005) due to a lack of discharge measurements. Wind and air temperature fields for the entire domain are provided with a spatial resolution of 0.0625° ($\sim 7 \text{ km}$) from 24-hour-forecasts at 1 hour time resolution (Deutscher Wetterdienst DWD). At the seaward open boundary, water level values stem from a numerical circulation model of the German Bight, the salinity value is kept constant at 32 psu and we

use water temperature values from the offshore observation station FINO1 (data from <http://fino.bsh.de>) which is located outside the model domain in the North Sea.

2.2 Scenario definitions

Two different bathymetric scenarios represent two states with different degrees of man-made modification: scenario “Hi” represents an actual, strongly impacted bathymetry. Scenario “Lo” represents a lesser impacted bathymetry, though far from being pristine. The modifications from Lo to Hi particularly include deepening and maintenance of the navigation channel, and silting of flood plains and side branches as related morphological reactions. Figure 2b and Figure 2c show that water depth in Hi is several meters larger compared to Lo in most sections of the navigation channel.

In Hi we use the bathymetry of the year 2010 as the most recent and consistent one available. In Lo, we replace the bathymetry in the section between the tidal barrier and km-120 by the 40 years older bathymetry of 1970. In the section of the replacement, bathymetry differences can be mainly attributed to anthropogenic modifications. The bathymetry of the estuarine mouth area further downstream was not changed in the model since there, bathymetric differences mainly result from natural morphologic changes. Note that the peculiar depth peak in scenario Lo at km-40 (Figure 2c) is due to the open construction of an immersed tube tunnel below the Elbe at that time.

We combine the two bathymetric scenarios Hi and Lo with four different discharge regimes, resulting in eight simulated scenarios, see Table 1: Hi-M and Lo-M include the variable, observed riverine freshwater discharge in the years 2010 and 2011. Hi-3 and Lo-3 run with a constant discharge of $300 \text{ m}^3 \text{ s}^{-1}$, corresponding to mean low summer discharge of $301 \text{ m}^3 \text{ s}^{-1}$ (FHH and HPA 2014). Hi-7 and Lo-7 (Hi-13 and Lo-13) run with $700 \text{ m}^3 \text{ s}^{-1}$ ($1300 \text{ m}^3 \text{ s}^{-1}$), corresponding to mean discharge of $713 \text{ m}^3 \text{ s}^{-1}$, and mean high summer discharge of $1280 \text{ m}^3 \text{ s}^{-1}$, respectively.

Table 1: Overview on scenarios; scenarios differ in bathymetry (Hi, Lo) and riverine freshwater inflow. The reference simulation Hi-M is based on the bathymetry Hi and measured riverine discharge; Hi-M thus represents the situation in the years 2010 and 2011.

Freshwater discharge	Measured 2010 – 2011	Constant $300 \text{ m}^3 \text{ s}^{-1}$	Constant $700 \text{ m}^3 \text{ s}^{-1}$	Constant $1300 \text{ m}^3 \text{ s}^{-1}$
Hi	Hi-M (reference)	Hi3	Hi7	Hi13
Lo	Lo-M	Lo3	Lo7	Lo13

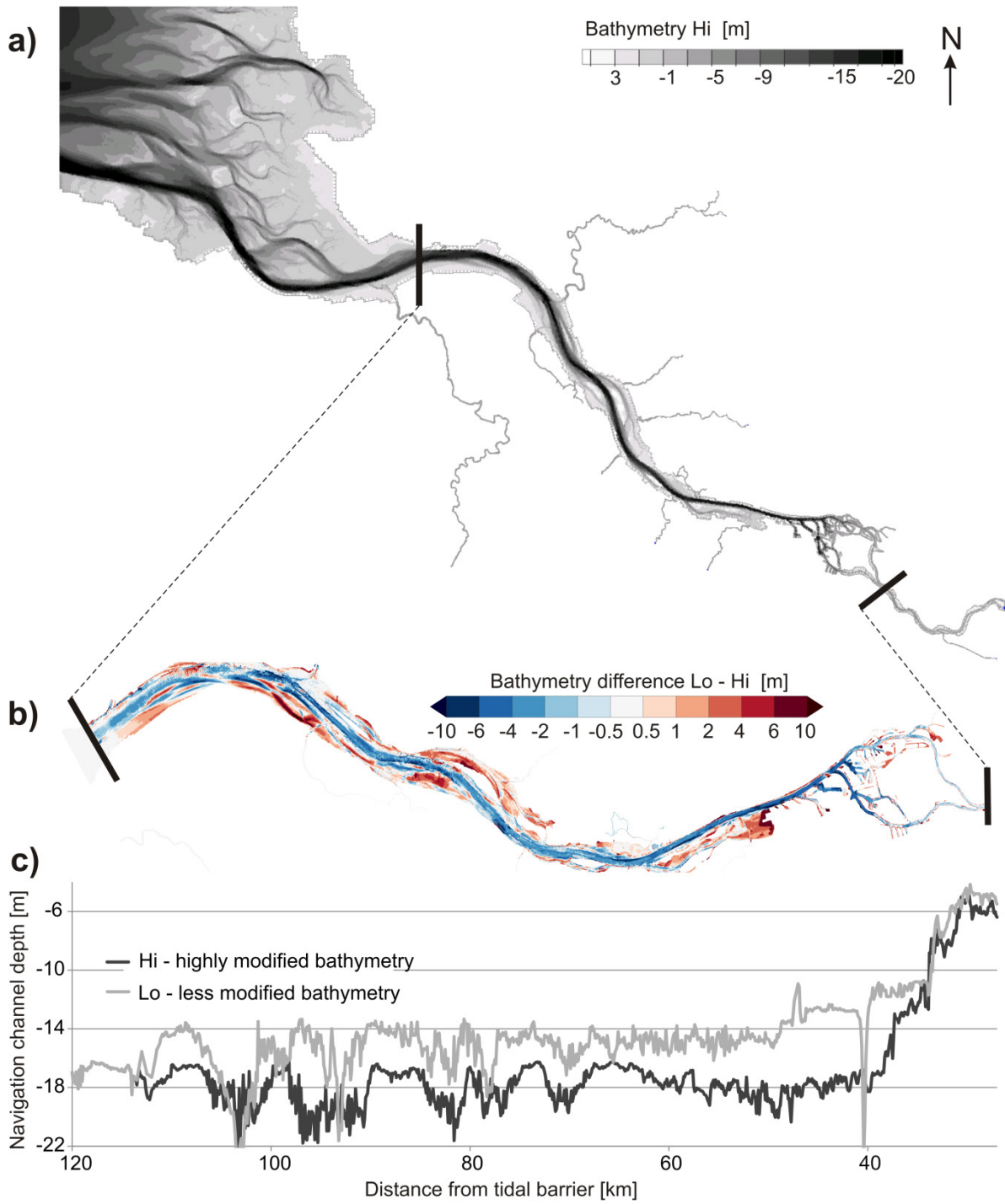


Figure 2: a) Model domain with bathymetry H_i , shown in the resolution as used in the subgrid bathymetry model. Thick black lines mark the section of largest bathymetry differences between H_i and Lo . b) Bathymetry difference $Lo - H_i$. Blue areas indicate that these parts are deeper whereas red areas are lower in the bathymetry H_i . c) Depth of the navigation channel along the estuary for the bathymetries H_i in black and Lo in grey.

2.3 Water age calculation

Delhez et al. (1999) defines the age of a water parcel as the time that elapsed since the water parcel entered a domain of interest outside of which the age is prescribed to be zero. Thereby, age is a pointwise, time-dependent result in the domain and its calculation is derived in an Eulerian framework to run with the algorithms of a numerical model.

We use the calculation of water age implemented in D-Water Quality (Postma et al. 2003, Smits and van Beek 2013), which is based on the tracking of two tracers that are transported by fluid motion. One tracer (T_{con}) is conservative whereas the other tracer (T_{dec}) is subjected to exponential growth or decay and related to the concentration of T_{con} according to: $C_{T_{dec}}(t) = C_{T_{con}} \cdot e^{-\gamma t}$.

The transport equations for the two tracers are

$$\frac{\partial C_{T_{con}}}{\partial t} = -\nabla \cdot (\mathbf{u} C_{T_{con}} - \mathbf{K} \nabla C_{T_{con}}) \quad (1)$$

$$\frac{\partial C_{T_{dec}}}{\partial t} = -\gamma C_{T_{dec}} - \nabla \cdot (\mathbf{u} C_{T_{dec}} - \mathbf{K} \nabla C_{T_{dec}}) \quad (2)$$

The water age a is then calculated by

$$a = \frac{\ln(C_{T_{dec}}/C_{T_{con}})}{-\gamma} \quad (3)$$

We focus on the age of riverine water because the riverine substance load governs the strong biogeochemical processes in the Elbe Estuary (Amann et al. 2012, 2012, 2014, 2014, Dähnke et al. 2008, Schroeder 1997). To estimate the time that elapsed since a riverine water signal entered the estuary, we charge water discharge at the tidal barrier with constant concentrations of the conservative as well as the decayable tracer. The decay rate of the decayable tracer is chosen to be $\gamma=0.01$ [d⁻¹]. During the simulation, riverine water age a_{riv} is then calculated for each computational element, based on Equation 3.

2.4 Calculation of hydraulic residence time

The hydraulic residence time t_{res} (Monsen et al. 2002; Zimmerman 1988), is defined as

$$t_{res} = V \cdot Q^{-1}, \quad (4)$$

where V is the estuarine volume upstream of a specific position, and Q is freshwater discharge. The definition of hydraulic residence time t_{res} in Equation (4) assumes stationary discharge and a completely mixed water volume.

Here, we determined t_{res} for the constant discharge scenarios Hi3, Hi7, and Hi13 by using the results of the hydrodynamic simulation for the calculation of V . We proceeded as follows: starting at the upstream model boundary (river boundary), we specified positions and corresponding cross sections every two kilometres downstream of each other. Solely the area where the estuary forms an inland delta and splits into a southern and northern stream, between km-22 and km-40, was not subdivided into smaller sections. The last cross section is located at km-114, where the estuarine funnel starts to open to the sea and extensive tidal flats are present. For each position, we calculated the upstream estuarine water volumes by summing up the water volumes of all computational cells located

upstream of the corresponding cross section. Finally, we averaged these aggregated water volumes over a spring-neap cycle.

This section-wise information on the average water volume for each constant discharge scenario was then used to calculate t_{res} along the estuary.

3 Results

3.1 Hydrodynamic model validity

Reference simulation (Hi-M) results demonstrate that the hydrodynamic model is capable of simulating the estuarine water movement with a good overall agreement between simulated cell values and point measurements. The skill for a direct comparison of simulated and observed values for water level, current velocity, salinity and water temperature is given in Table 2 and Figure 3. For the skill assessment of water level, we used data from 14 observation stations, which were provided by the German Water and Shipping Administration. From upstream to downstream, these are the stations Altengamme, Over, Bunthaus, Hamburg St. Pauli, Seemannshoef, Schulau, Hetlingen, Stadersand, Grauerort, Glueckstadt, Brokdorf, Cuxhaven, Scharhoern and Bake A. For the skill assessment of current velocity, salinity and water temperature, we compared depth averaged model results to the observational values. For the stations D1 Hanskalbsand, D2 Julesand, D3 Pagensand, D4 Rhinplate (Water and Shipping Administration), which are equipped with a fixed bottom sensor and a vertically moving top sensor 0.8 m below the water surface, observational values were also depth averaged. In addition to these four stations, the stations LZ1a, LZ1, LZ1b, LZ2, LZ3 and LZ4 (Water and Shipping Administration) were included in the skill assessment for salinity and water temperature, and Bunthaus, Seemannshoef and Blankenese (Institut fuer Hygiene und Umwelt Hamburg, www.wgmn.hamburg.de, license dl-de/by-2-0) for water temperature. Refer to Figure 1 for the positions of all observation stations.

Table 2: Model skill in comparison to observations. n gives the number of observation stations. The statistical figures were calculated using all available measurements at each station for the entire simulation period from 01.01.2010 to 31.12.2011.

Variable with n = number of stations	Mean correlation	Mean difference	Root mean square error
Water level (n=14)	0.99	0.10 (m)	0.15 (m)
Current velocity (n=4)	0.930	0.11 (m/s)	0.12 (m/s)
Salinity (n=10)	0.867	2.10 (psu)	2.4 (psu)
Water temperature (n=12)	0.991	0.97 (°C)	1.23 (°C)

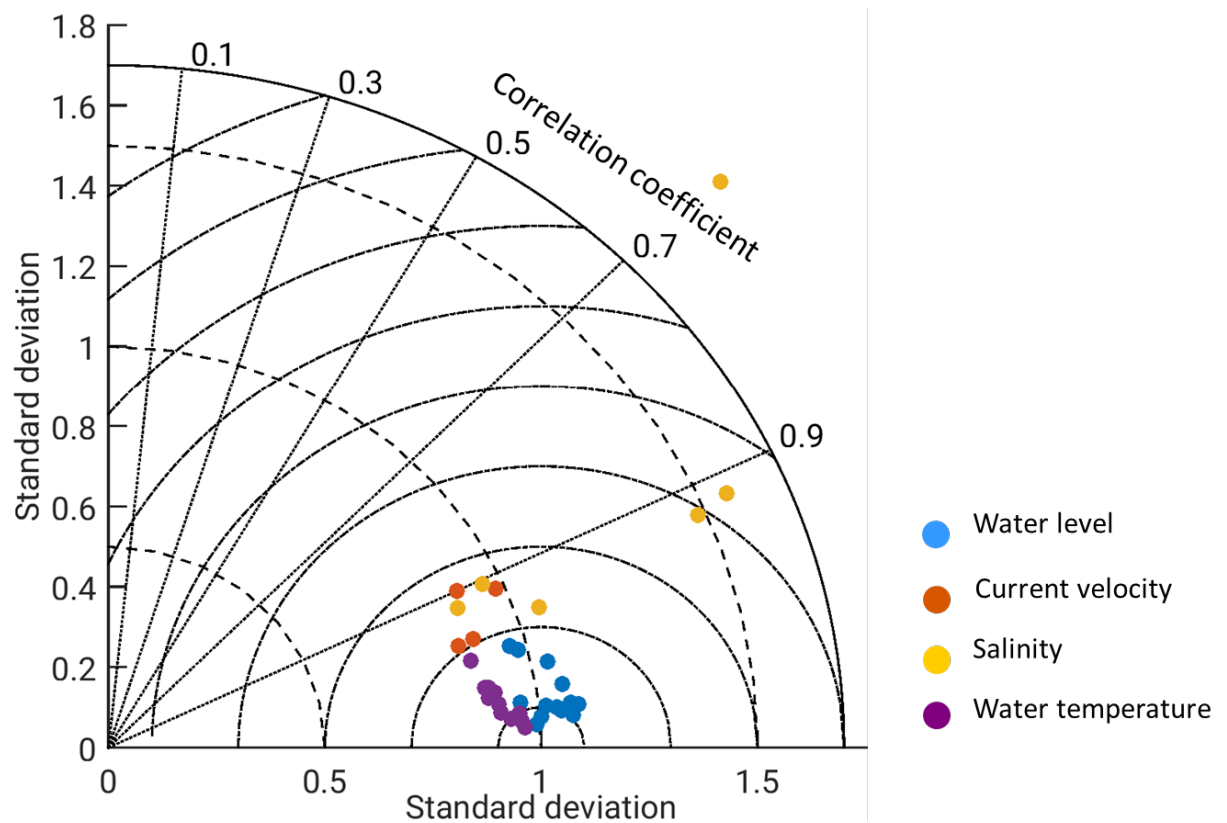


Figure 3: Normalized Taylor diagram on the statistical comparison of model results for the reference scenario Hi-M to observations. Blue dots show values for model skill at the positions of water level measurements, red dots for current velocities, yellow dots for salinity and violet dots for water temperature. Observation stations and period of comparison are identical to the ones assessed in Table 2.

Time series comparison generally shows a good agreement between simulated and observed water level and current velocity, including magnitude and timing, see two examples in Figure 4 with a) at a position in the beginning of the salinity gradient zone, and b) at a position in the freshwater zone, i.e. the section of the estuary where salinity is only determined by riverine salinity. However, the main shortcoming of the model is the intrusion of salinity too far upstream, as can be seen in Figure 4 a): at the upstream end of the salt mixing zone, the model overestimates salinity with 2 to 3 psu. The salinity stations which show the noticeable poor skill in Figure 3 are located in this region. The deviation in water temperature predominantly occurs during summer and mainly originates from neglecting the effect of power plant cooling waters.

The differences in tidal characteristic numbers of water level, see Table 3, show that overall, the tidal curve is modeled with an 18 cm too large tidal range, which is almost equally distributed between an overestimated high water level and an underestimated low water level. High water and low water occur roughly 10 minutes later in the simulation, while differences in the duration of flood period and ebb period are below one minute. Our results complement (Sehili et al. 2014) who already showed good agreement between model results and observations for water level during selected periods in the years 2006 and 2011. Altogether, the model provides a reliable hydrodynamic base.

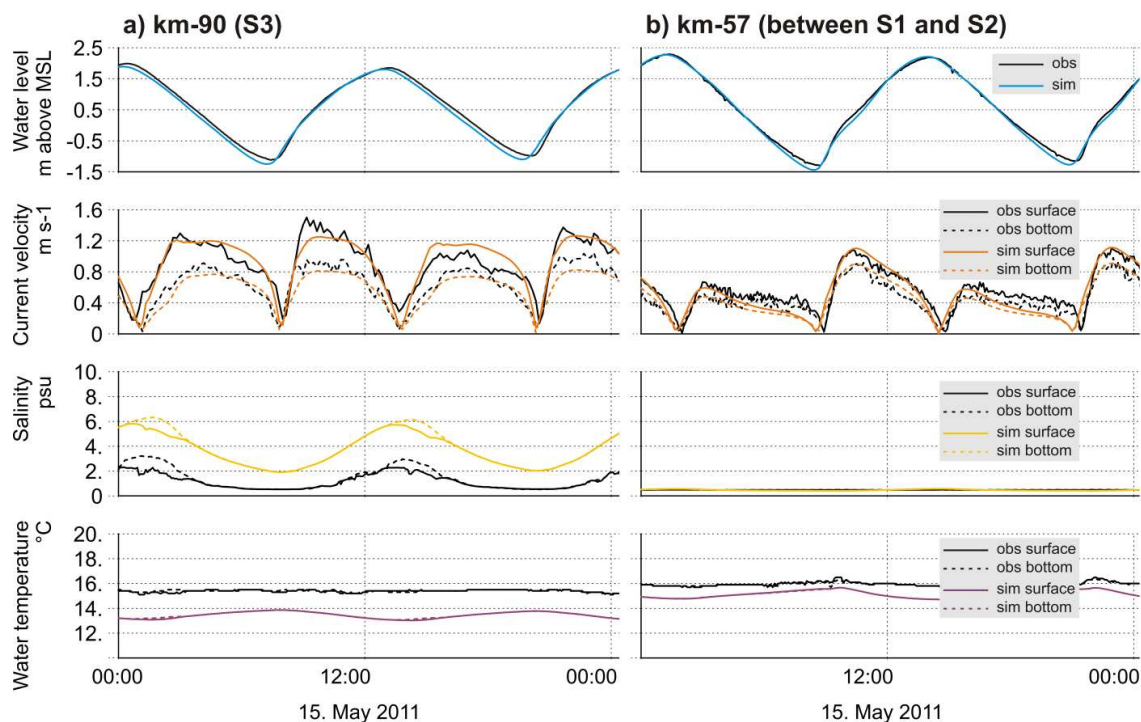


Figure 4: Time series comparison of observed and simulated water level, current velocity, salinity and water temperature; a) at position km-90 with water level measured at Glueckstadt, and current velocity, salinity and water temperature measured at D4 Rhinplate; b) at position km-57 with water level measured at Schulau, and current velocity, salinity and water temperature measured at D1 Hanskalbsand.

Table 3: Differences in tidal characteristic numbers of water level between simulated results and observational data (sim – obs) for the period 01.02.2010 to 31.12.2011, including 1349 tidal cycles at 14 observation stations. Second column contains the mean difference over all stations, with the mean values of absolute differences given in brackets. We used the postprocessors ncanalyse and ncdelta for the analysis (<http://wiki.baw.de/en/index.php/NCANALYSE> and <http://wiki.baw.de/en/index.php/NCDELTA>).

Difference in	Mean (abs(mean))	Min	Max
Mean high water level [m]	+ 0.09 (0.11)	- 0.01 (Cuxhaven)	+ 0.21 (Bunthaus)
Mean low water level [m]	- 0.09 (0.10)	- 0.02 (Cuxhaven)	- 0.19 (Altengamme)
Mean tidal range [m]	+ 0.18 (0.19)	+ 0.01 (Bake A)	+ 0.37 (Altengamme)
Mean water level [m]	+ 0.01 (0.03)	- 0.07 (Bake A)	+ 0.06 (Hetlingen)
Time of high water [min]	+ 12.0 (12.3)	-1 (Cuxhaven)	+ 20 (Grauerort)
Time of low water [min]	+ 7.8 (8.8)	-6 (Cuxhaven)	+ 21 (Altengamme)
Flood period duration [min]	- 0.5 (3.5)	-15 (Altengamme)	+ 6 (Grauerort)
Ebb period duration [min]	+ 0.3 (3.8)	- 5 (Grauerort)	+ 16 (Altengamme)
Flood mean water level [m]	- 0.03 (0.04)	- 0.08 (Grauerort)	+ 0.01 (Altengamme)
Ebb mean water level [m]	+ 0.04 (0.06)	- 0.09 (Bake A)	+ 0.11 (Hetlingen)

3.2 Reference water age

In the reference scenario Hi-M, riverine water age a_{riv} generally increases from upstream to downstream: Figure 5a shows a_{riv} during the year 2011 at three stations S1, S2, S3 along the estuarine shipping channel (positions marked in Figure 1) with S1 being the most upstream station and having smaller a_{riv} values than S2 than S3. The areal overview confirms that a_{riv} increases downstream, see Figure 6a, which shows spring-neap averaged a_{riv} values during low river discharge condition.

Riverine water age a_{riv} exhibits a strong dependency on river discharge (blue line in Figure 5a): after the high discharge event at the end of January, a_{riv} values are smallest for all stations (e.g. 0.9 days at S1, 3.8 days at S3) while values are largest in July after several weeks of low discharge (e.g. 9.1 days at S1, 25.2 days at S3). The further downstream the station, the bigger is the difference between smallest a_{riv} after high discharge and largest a_{riv} during low discharge: while this difference is about 8 days at S1, it is more than 20 days at S3. The a_{riv} difference between the stations also depends on discharge, e.g. the a_{riv} difference between S1 and S3 after the peak discharge in January is about 3 days whereas it is more than 15 days during the low flow period in June/July.

When looking at a_{riv} values in dependence on river discharge without chronological allocation (dots in Figure 5b), the behavior described above appears even more consistent: at similar discharge, a_{riv} values are larger the further downstream the station; at the same station, a_{riv} values are larger the smaller the discharge; the further downstream the station, the larger the a_{riv} difference at high discharge compared to low discharge; and, finally, the lower the discharge, the higher the a_{riv} differences between upstream and downstream stations.

At each station, a_{riv} seems to be inversely proportional to river discharge Q ; Figure 5b displays a fitted line at each station S1 to S3 of a_{riv} in dependence of Q^{-1} .

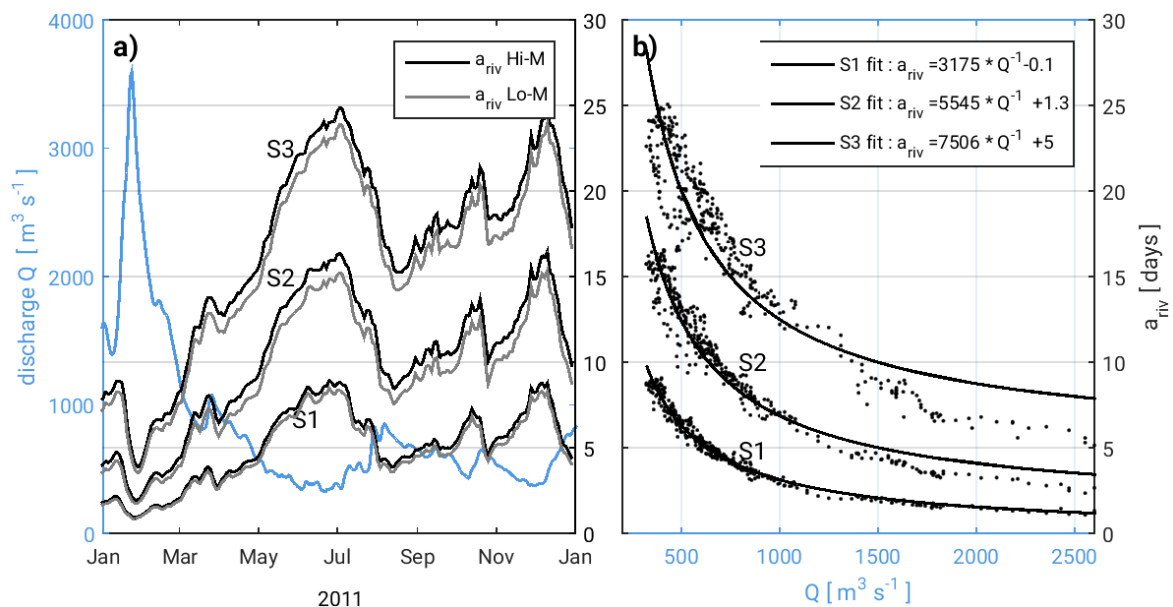


Figure 5: a) Time series of measured river discharge Q (blue line) and calculated, tidally averaged riverine water age a_{riv} for the year 2011. Values for a_{riv} are shown at the stations S1 (km-43, position Seemannshöft) and S2 (km-65, D2 Julesand) in the estuarine freshwater part, and S3 (km-90, position D4 Rhinplate) in the salinity mixing zone for the scenarios Hi-M (black) and Lo-M (grey), respectively. b) Black dots show daily a_{riv} values plotted versus freshwater discharge Q for the stations S1, S2 and S3; the lines show a fit for each station with the equation given in the box.

3.3 Water age for bathymetric and constant discharge scenarios

In scenario Lo-M, a_{riv} is usually smaller compared to Hi-M, see in Figure 5a grey lines compared to black lines. The differences are in the order of hours at S1, S2, and S3, and thus lower than the differences caused by the natural variability of river discharge. At S1, the difference in a_{riv} between the two scenarios Hi-M and Lo-M is smallest following the flood event (~ 1 hour difference) and highest during the low-flow period (~ 14 hours difference). At S3, differences are larger but behave in the same way: differences are smallest after the flood in January (~ 8 hours difference) and they are highest during low river discharge (~ 38 hours).

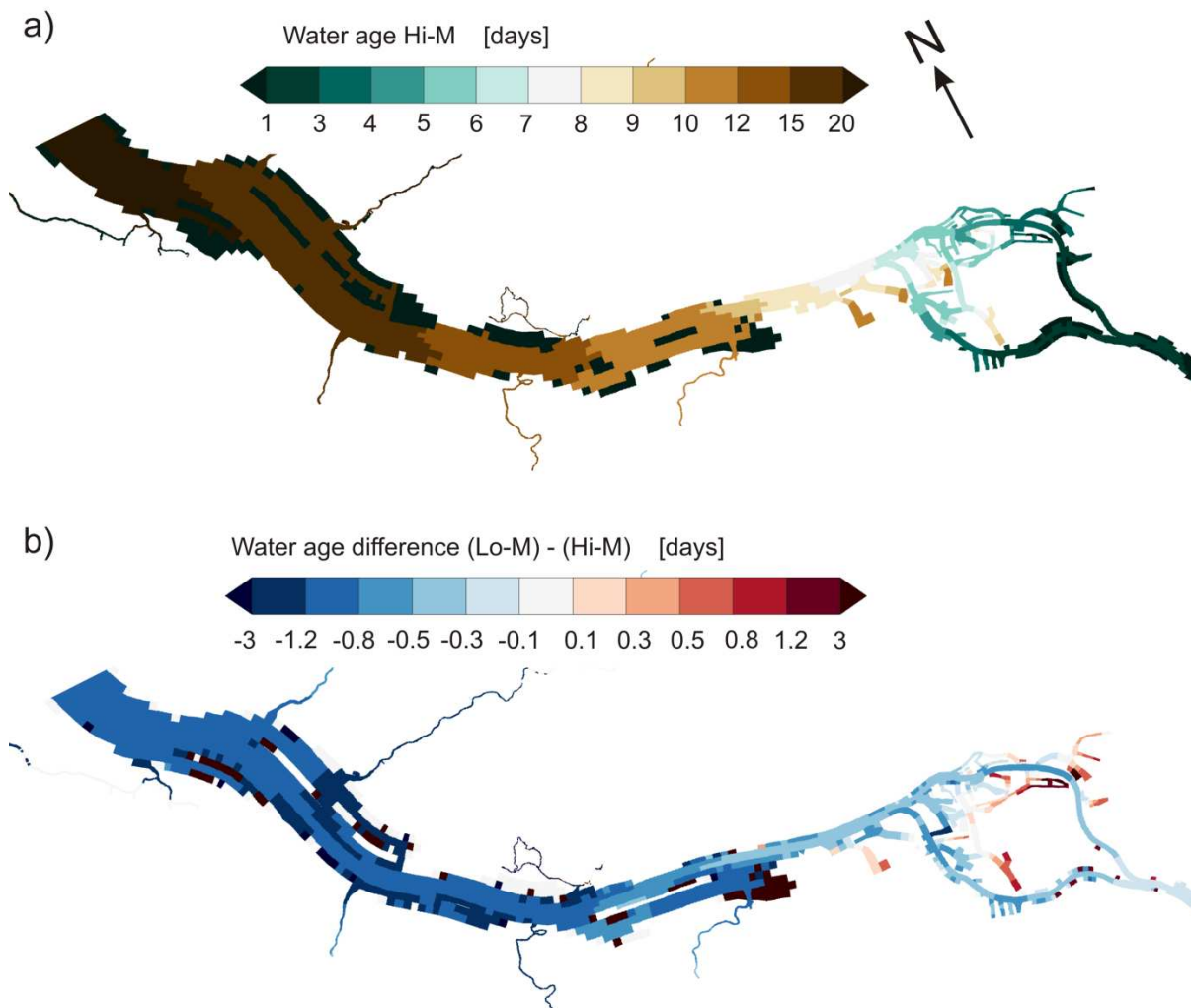


Figure 6: a) Spring-neap tidally averaged water age a_{riv} in June 2011 for scenario Hi-M. There are some conspicuous patches in the middle of the estuary (sand banks and islands) and at the banks that appear to have a water age below 1 day: these are elevated areas that have fallen dry and have a water age of zero. b) Water age difference (Lo-M) - (Hi-M) of spring-neap tidally averaged water age for boundary conditions of June 2011. Similar to a), there are patches where water age difference above 3 days is displayed: these areas fell dry in Hi-M but not in Lo-M, leading to the apparently high difference.

The areal differences between Hi-M and Lo-M (Figure 6b) confirm that a_{riv} is larger in Hi-M, apart from some harbor basins and bank areas that silted up or had been backfilled. Figure 6b also indicates that a_{riv} differences increase downstream.

In the constant freshwater discharge scenarios (Hi3, Hi7, Hi13), riverine water age a_{riv} behaves similarly to the scenarios with variable, measured discharge: a_{riv} increases with distance from the tidal barrier and with decreasing discharge (Figure 7 upper left panel). In addition to the variable discharge scenarios, the quasi-stationary results for the constant discharge scenarios better allow an evaluation on the longitudinal profile. Most prominent is the accelerated increase in a_{riv} between km-20 and km-35 (Figure 7 zoom area on upper right panel). During the 15 km long distance, a_{riv} increases from 1.5 days to 6.4 days in the low-flow scenario Hi3, from 14 hours to 2.5 days in Hi7 and from 8 hours to 1.3 days in Hi13. Downstream of km-35, the increase in a_{riv} continues steadily but more gradually. 55 km further downstream, at position S3, a_{riv} reaches values of 24.8 days in Hi3, of 15.6 days in Hi7 and of 9.5 days in Hi13.

Water age in the corresponding Lo constant discharge scenarios is always smaller (Figure 7 upper panels, flat-colored lines for Lo-scenarios in comparison to intensely-colored lines for Hi-scenarios). However, differences are in the order of a few hours up to 1 day maximum (see Figure 7 lower panels). While a_{riv} differences between Hi7 and Lo7, and Hi13 and Lo13, grow almost continuously from upstream to downstream until km-70 in Lo7 and until km-100 in Lo13, the differences between Hi3 and Lo3 peak twice along the estuary: at around km-30 where a_{riv} is 16 hours smaller, and second between km-60 and km-80 where it is almost 1 day smaller in the shallower bathymetry Lo. Downstream of km-80, a_{riv} values in Hi3 and Lo3 converge whereas differences in Hi7/Lo7, Hi13/Lo13 respectively, appear to remain almost constant until km-140.

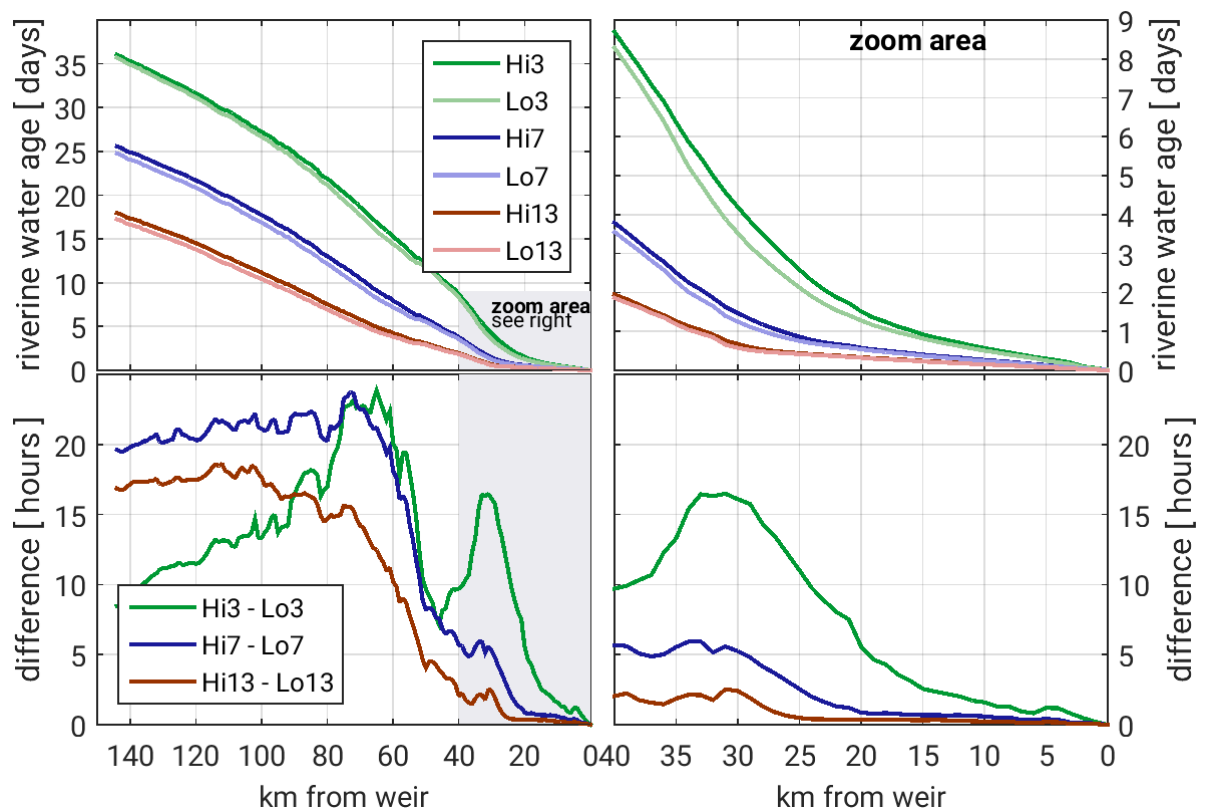


Figure 7: Upper panels: Riverine water age along the estuary for scenarios with constant discharge. Lower panels: Difference in riverine water age between scenarios with the same discharge but different bathymetries. Left panels show values along the entire shipping channel, right panels show a zoom in the upstream 40 km of the shipping channel.

4 Discussion

4.1 Relation between water age and river discharge

Riverine water age a_{riv} is determined by river discharge (Figure 5). The dependency between a_{riv} and Q is clearest at the most upstream position S1 and, because of a delayed response, becomes less distinct further downstream: the effect of a change in Q needs some time to propagate through the system and the assumption of fast/instantaneous adaptation of a_{riv} becomes less precise the more downstream the location of interest. This delayed response also causes the difference at high discharge values between a_{riv} and the fitted line in Figure 5 b), which is particularly evident for the position S3. A possibility for a better fit was to relate the riverine water age $a_{riv}(x,t)$ at an arbitrary position x downstream of the discharge ($x = 0$) and at an arbitrary point in time t to the entire discharge history between $t - a_{riv}(x,t)$ and t . However, the capability to predict a_{riv} would be lost by using such a relationship.

The observed inverse proportionality between a_{riv} and Q (Figure 5 b) can be explained by the hydraulic residence time t_{res} : Figure 8 shows both transport time scales, a_{riv} and t_{res} , for the constant discharge scenarios on the actual, strongly impacted bathymetry. For each discharge scenario, the two transport time scales are similar in the freshwater region. The differences are in the range of hours between the hydraulic residence time t_{res} , which constitutes an integral measure for the entire water volume upstream of a specific position, and riverine water age a_{riv} , which gives a local value. Their similarity illustrates the well-mixed nature of the freshwater zone and demonstrates that a_{riv} is mainly driven by downstream-oriented residual flow which is induced by discharge.

It has to be noted that the limit of the freshwater region depends on discharge and migrates upstream with decreasing discharge. The model simulates the freshwater limit at around km-55 for a constantly low discharge of $300 \text{ m}^3 \text{ s}^{-1}$ (in Scenario Hi3), at km-85 in Hi7, and at km-105 in Hi13. However, the salt front in the model penetrates too far landwards, see Figure 4, so the above given limits of the freshwater region can be expected to be located several kilometres further downstream.

Downstream of the freshwater region, the two transport time scales increasingly deviate from each other, mainly because of two reasons: first and foremost, the volume V in Equation (4) is progressively filled with seawater instead of water that originates from river discharge. Second, the underlying assumption in Equation (4) of a completely mixed water volume becomes continuously less valid with downstream position.

In contrast to t_{res} , a_{riv} remains a valid transport time scale for river water throughout the estuary because it gives the time that has elapsed since the water entered the estuary at the upstream boundary, independent of the ratio of freshwater to seawater and under varying discharge.

So far, the concept of water age has mainly been applied in systems characterized by stratification, and a strong dependency of water age on discharge has also been found in these systems. There, in addition to a general decrease in water age with increasing discharge, an influence is also given by a larger vertical difference between smaller age values at the surface and larger age values at the bottom (Kärnä and Baptista 2016, Ren et al. 2014, Shen and Lin 2006). Apart from discharge, tidal forcing (Shen and Lin 2006) and wind (Gong et al. 2009) have been described to influence the vertical distribution of age in stratified systems.

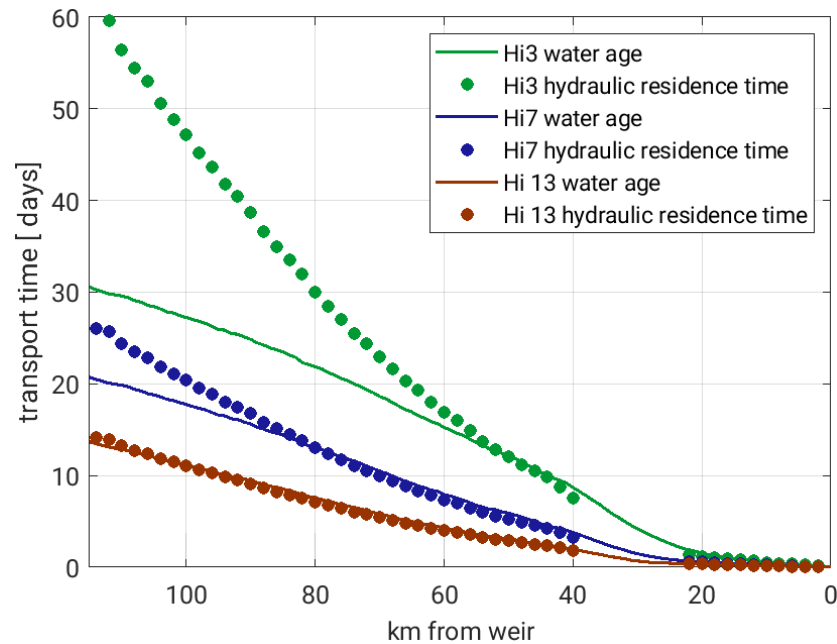


Figure 8: Riverine water age (solid lines) and hydraulic residence times (dots) for the constant discharge scenarios Hi3 (green), Hi7 (blue) and Hi13 (red) along the shipping channel. The gap in hydraulic residence time data between km-22 and km-40 is because the inland delta in that area has not been divided into separate sections for the analysis of water volume.

4.2 Effect of man-made bathymetric modification on water age

The variation in water age a_{riv} due to varying discharge within each of the scenarios Hi-M and Lo-M is much larger than the difference in a_{riv} due to a different bathymetry at any equal discharge regime, although large depth differences exist between the bathymetric scenarios Hi and Lo (Figure 2b and Figure 2c). In scenario Hi, the navigation channel is several meters deeper whereas lateral areas at the banks of the estuary are up to several meters shallower. In total, the estuarine volume is about 6.7 % larger in Hi compared to Lo. The larger water volume explains the general increase in riverine water age under the higher human impact in Hi-M.

During the time period that we considered in this study, discharge values were not constant long enough for a_{riv} to reach steady state values. We therefore also studied scenarios with different constant discharges and found the a_{riv} differences between the bathymetric scenarios (Hi3 and Lo3, Hi7 and Lo7, Hi13 and Lo13, respectively) to be in the same order of magnitude as the difference between Hi-M and Lo-M. This consistency in results for different discharge regimes lets us reliably determine the difference in a_{riv} due to the bathymetric modifications to be in the order of several hours in most sections of the estuary, corresponding to 6–8 % of the absolute value. This relative increase in riverine water age in the higher impacted bathymetry corresponds to the relative increase in water volume. Thus, the difference in riverine water age can also be explained quantitatively by the increase in volume, considering the similarity to hydraulic residence time: in Equation (4), a variation in volume directly changes t_{res} by the same relative amount.

This almost direct quantitative dependency between a change in water volume and a change in age can be expected to be generally applicable to well-mixed estuaries, or well-mixed sections of otherwise more stratified estuaries. In contrast, in stratified estuaries,

where a vertical variability in age and other additional influences apart from discharge on the vertical age distribution play a role, a more complex relation may exist.

4.3 Relation to estuarine oxygen dynamics

Transport time scales are usually explored in the context of biogeochemical or water quality issues (Ahmed et al. 2017, Brye et al. 2012, Chan et al. 2002, Fujiwara et al. 2002, Rayson et al. 2016, Shen and Haas 2004). Here, we focus on estuarine oxygen dynamics because in the Elbe Estuary (Amann et al. 2012, Schroeder 1997) and in many other contemporary estuaries worldwide, estuarine oxygen minimum zones (eOMZs) are frequently observed (Abril et al. 2003, Billen et al. 2001, Hagy et al. 2004, Ruiz et al. 2015, Tomaso and Najjar 2015, Zhang and Li 2010). The eOMZs are mainly linked to anthropogenic impacts, of which eutrophication is the most frequently reported cause (Breitburg et al. 2003, Cloern 2001, Conley et al. 2009, Diaz 2001, Díaz and Rosenberg 2011, Howarth et al. 2011, Kemp et al. 2009, Paerl 2006, 2009, Rabalais et al. 2010): the increase in land-borne nutrients due to the wash out of agricultural fertilizers increases primary production in the limnic river sections which transforms into labile detritus when reaching the deeper and more turbid estuarine sections. Bacterial respiration of such easily degradable detritus consumes oxygen and results in an eOMZ if the oxygen depletion cannot be counterbalanced by atmospheric reaeration or primary production.

Generally, physical and biogeochemical processes interact in the formation and control of eOMZs (Du and Shen 2015, Kemp and Boynton 1980). Previous studies have attempted to estimate the effect of physical processes on eOMZs, mainly for stratified and partially stratified estuaries (Bruce et al. 2014, Du and Shen 2015, Fujiwara et al. 2002, Scully 2013), where wind conditions and freshwater discharge govern the strength of the stratification and thus are the dominating physical influence mechanisms. For well-mixed estuaries, comparable studies are missing, maybe because the intrinsic hydrodynamic conditions are favourable to counteract low dissolved oxygen concentrations by the generally greater possibility to supply oxygenated water from the surface. Nevertheless, eOMZs regularly occur in many well-mixed estuaries (Diez-Minguito et al. 2014, Lanoux et al. 2013, Schroeder 1997, Verity et al. 2006).

Bathymetric deepening in well-mixed estuaries influences physical factors of eOMZ formation, mainly the transport of degradable organic matter via changes in hydrodynamics and the relative atmospheric interface for reaeration due to the reduction in water surface-to-volume ratio. Despite these possible influences of bathymetric deepening on an eOMZ, there is no quantification of physical effects known to us, though, similar to the Elbe Estuary, many well-mixed estuaries worldwide experience the phenomena of a strongly deepened navigation channel and severe eOMZs, like the upper Delaware Estuary (DiLorenzo et al. 1994, Sharp 2010, Tomaso and Najjar 2015), the Scheldt (Meire et al. 2005, van Damme et al. 2005), the Loire (Abril et al. 2003, Etcheber et al. 2007, Walther et al. 2015) or the Guadalquivir (Diez-Minguito et al. 2014, Ruiz et al. 2015).

The time it takes for degradable organic matter to be transported to a specific location determines the completeness of its heterotrophic degradation. Middelburg and Herman (2007), for example, showed that organic matter is extensively modified due to heterotrophic processing in estuaries with long residence times compared to estuaries with shorter residence times. An analysis in Lanoux et al. (2013) for the Gironde estuary hints at lower

oxygen concentration during a period of longer residence times compared to a period of shorter residence time under otherwise similar environmental conditions. It is thus a plausible concept that a longer transport time induces higher accumulated oxygen consumption between the origin of degradable organic matter and some specific location.

Given the detected increase in a_{riv} of approximately 7 %, our results hint at an increase in accumulated oxygen demand caused by a realistic, 40-year bathymetric change due to human interference. If the higher oxygen consumption will also finally lead to a more severe eOMZ, strongly depends on the possibility for reaeration (Holzwarth and Wirtz 2018).

5 Conclusion

This is the first study on the impact of a bathymetry difference on riverine transport time scale in an estuary. We show for the Elbe Estuary that the effect of a bathymetric difference, which reflects a realistic 40-year impact of typical man-made modification, on riverine water age is much smaller than the effect of the natural, seasonal variability in river discharge. The age difference between the bathymetric scenarios lies in the order of hours up to one day maximum, depending on location and discharge. This difference corresponds to a 6–8 % larger relative riverine water age in the bathymetry with higher human impact.

Due to the well-mixed character of the Elbe Estuary, this increase in riverine water age is mainly caused by the increase in water volume, and an almost direct quantitative dependency between a change in water volume and a change in age exists.

Generally, riverine water age in the Elbe Estuary is governed by river discharge; the age is small after time intervals with high discharges and increases, proportional to the inverse of discharge, during periods of low discharge. Thereby, the age difference between highest and lowest discharge is in the order of days for upstream stations and grows to weeks for stations in the salinity gradient zone.

Notwithstanding the apparently small impact, the effect of the larger water age in the higher impacted bathymetry potentially leads to higher accumulated oxygen consumption. In combination with reduced oxygen reaeration due to the decreased water surface-to-volume ratio, the higher impacted bathymetry generates additional stressors to the estuarine oxygen minimum zone, acting into the direction of lower oxygen levels. We thus expect hydrodynamic effects by bathymetry deepening to intensify the eutrophication impact on estuarine oxygen levels.

6 Acknowledgements

We thank Frank Böker (BAW) for preparing the different model bathymetries and Günther Lang (BAW) for his valuable input on the hydrodynamic simulations and the postprocessing of the results.

The work of Ingrid Holzwarth and Holger Weilbeer was funded as part of the Federal Waterways Engineering and Research Institute (BAW) departmental research and development program. The work of Kai W. Wirtz was supported by the German Federal Ministry of Education and Research (BMBF) through the MOSSCO project and by the Helmholtz Society through the PACES program.

7 References

- Abood, K. A.; Metzger, S. G.; Distant, D. F.: Minimizing Dredging Disposal via Sediment Management in New York Harbor. In: *Estuaries*, 22, 3, 763, 1999.
- Abril, G.; Etcheber, H.; Delille, B.; Frankignoulle, M.; Borges, A. V.: Carbonate dissolution in the turbid and eutrophic Loire estuary. In: *Marine Ecology Progress Series*, 259, 129–138, 2003.
- Ahmed, A.; Pelletier, G.; Roberts, M.: South Puget Sound flushing times and residual flows. In: *Estuarine, Coastal and Shelf Science*, 187, 9–21, 2017.
- Amann, T.; Weiss, A.; Hartmann, J.: Carbon dynamics in the freshwater part of the Elbe estuary, Germany: Implications of improving water quality. In: *Estuarine, Coastal and Shelf Science*, 107, 112–121, 2012.
- Amann, T.; Weiss, A.; Hartmann, J.: Silica fluxes in the inner Elbe Estuary, Germany. In: *Biogeochemistry*, 118, 1–3, 389–412, 2014.
- Avoine, J.; Allen, G. P.; Nichols, M.; Salomon, J. C.; Larssonneur, C.: Suspended-sediment transport in the Seine estuary, France. Effect of man-made modifications on estuary-shelf sedimentology. In: *Marine Geology*, 40, 1–2, 119–137, 1981.
- Bergemann, M.; Blöcker, G.; Harms, H.; Kerner, M.; Meyer-Niehl, R.; Petersen, W.; Schroeder, F.: Der Sauerstoffhaushalt der Tideelbe. In: *Die Küste*, 58, 199–261, 1996.
- Billen, G.; Garnier, J.; Ficht, A.; Cun, C.: Modeling the response of water quality in the Seine River Estuary to human activity in its watershed over the last 50 years. In: *Estuaries*, 24, 6, 977, 2001.
- Breitburg, D. L.; Adamack, A.; Rose, K. A.; Kolesar, S. E.; Decker, B.; Purcell, J. E.; Keister, J. E.; Cowan, J. H.: The pattern and influence of low dissolved oxygen in the Patuxent River, a seasonally hypoxic estuary. In: *Estuaries*, 26, 2, 280–297, 2003.
- Bruce, L. C.; Cook, P. L. M.; Teakle, I.; Hipsey, M. R.: Hydrodynamic controls on oxygen dynamics in a riverine salt wedge estuary, the Yarra River estuary, Australia. In: *Hydrology and Earth System Sciences*, 18, 4, 1397–1411, 2014.
- Brye, B. de; Brauwere, A. de; Gourgue, O.; Delhez, E. J.M.; Deleersnijder, E.: Water renewal timescales in the Scheldt Estuary. In: *Journal of Marine Systems*, 94, 74–86, 2012.
- Casulli, V.: A high-resolution wetting and drying algorithm for free-surface hydrodynamics. In: *International Journal for Numerical Methods in Fluids*, 60, 4, 391–408, 2009.
- Casulli, V.; Stelling, G. S.: Semi-implicit subgrid modelling of three-dimensional free-surface flows. In: *International Journal for Numerical Methods in Fluids*, 67, 4, 441–449, 2010.
- Chan, T. U.; Hamilton, D. P.; Robson, B. J.; Hodges, B. R.; Dallimore, C.: Impacts of hydrological changes on phytoplankton succession in the Swan River, Western Australia. In: *Estuaries*, 25, 6, 1406–1415, 2002.
- Cloern, J. E.: Our evolving conceptual model of the coastal eutrophication problem. In: *Marine Ecology Progress Series*, 210, 223–253, 2001.

- Conley, D. J.; Paerl, H. W.; Howarth, R. W.; Boesch, D. F.; Seitzinger, S. P.; Havens, K. E.; Lancelot, C.; Likens, G. E.: Ecology. Controlling eutrophication. Nitrogen and phosphorus. In: *Science* (New York, N.Y.), 323, 5917, 1014–1015, 2009.
- Dähnke, K.; Bahlmann, E.; Emeis, K.: A nitrate sink in estuaries? An assessment by means of stable nitrate isotopes in the Elbe estuary. In: *Limnology and Oceanography*, 53, 4, 1504–1511, 2008.
- Deleersnijder, E.; Campin, J.-M.; Delhez, E. J. M.: The concept of age in marine modelling. In: *Journal of Marine Systems*, 28, 3–4, 229–267, 2001.
- Delhez, E. J.M.; Campin, J.-M.; Hirst, A. C.; Deleersnijder, E.: Toward a general theory of the age in ocean modelling. In: *Ocean Modelling*, 1, 1, 17–27, 1999.
- Delhez, É. J.M.; Brye, B. de; Brauwere, A. de; Deleersnijder, É.: Residence time vs influence time. In: *Journal of Marine Systems*, 132, 185–195, 2014.
- Delhez, É. J.M.; Deleersnijder, É.: The concept of age in marine modelling. In: *Journal of Marine Systems*, 31, 4, 279–297, 2002.
- Delhez, É. J.M.; Lacroix, G.; Deleersnijder, É.: The age as a diagnostic of the dynamics of marine ecosystem models. In: *Ocean Dynamics*, 54, 2, 221–231, 2004.
- Díaz, R. J.: Overview of hypoxia around the world. In: *Journal of Environment Quality*, 30, 2, 275, 2001.
- Díaz, R. J.; Rosenberg, R.: Introduction to Environmental and Economic Consequences of Hypoxia. In: *International Journal of Water Resources Development*, 27, 1, 71–82, 2011.
- Diez-Minguito, M.; Baquerizo, A.; Swart, H. E. de; Losada, M. A.: Structure of the turbidity field in the Guadalquivir estuary. Analysis of observations and a box model approach. In: *Journal of Geophysical Research: Oceans*, 119, 10, 7190–7204, 2014.
- DiLorenzo, J. L.; Huang, P.; Thatcher, M. L.; Najarian, T. O.: Dredging Impacts on Delaware Estuary Tides. In: Spaulding, M. L. (ed.): *Proceedings of the 3rd international conference / 3rd International Conference on Estuarine and Coastal Modeling*. Oak Brook, Illinois, September 8–10, 1993, American Soc. of Civil Engineers, New York, NY, 1994.
- Du, J.; Shen, J.: Decoupling the influence of biological and physical processes on the dissolved oxygen in the Chesapeake Bay. In: *Journal of Geophysical Research: Oceans*, 120, 1, 78–93, 2015.
- Ensing, E.; Swart, H. E. de; Schuttelaars, H. M.: Sensitivity of tidal motion in well-mixed estuaries to cross-sectional shape, deepening, and sea level rise. In: *Ocean Dynamics*, 65, 7, 933–950, 2015.
- Etcheber, H.; Taillez, A.; Abril, G.; Garnier, J.; Servais, P.; Moatar, F.; Commarieu, M.-V.: Particulate organic carbon in the estuarine turbidity maxima of the Gironde, Loire and Seine estuaries: Origin and lability. In: *Hydrobiologia*, 588, 1, 245–259, 2007.
- FHH; HPA: *Deutsches gewässerkundliches Jahrbuch. Elbegebiet, Teil III: Untere Elbe ab der Havelmündung*. In German, Hamburg, 2014.

- Fujiwara, T.; Takahashi, T.; Kasai, A.; Sugiyama, Y.; Kuno, M.: The role of circulation in the development of hypoxia in Ise Bay, Japan. In: *Estuarine, Coastal and Shelf Science*, 54, 1, 19–31, 2002.
- Geyer, W. R.; MacCready, P.: The Estuarine Circulation. In: *Annual Review of Fluid Mechanics*, 46, 1, 175–197, 2014.
- Gong, W.; Shen, J.; Hong, B.: The influence of wind on the water age in the tidal Rappahannock River. In: *Marine Environmental Research*, 68, 4, 203–216, 2009.
- Hagy, J. D.; Boynton, W. R.; Keefe, C. W.; Wood, K. V.: Hypoxia in Chesapeake Bay, 1950–2001. Long-term change in relation to nutrient loading and river flow. In: *Estuaries*, 27, 4, 634–658, 2004.
- Holzwarth, I.; Wirtz, K.: Anthropogenic impacts on estuarine oxygen dynamics. A model based evaluation. In: *Estuarine, Coastal and Shelf Science*, 211, 45–61, 2018.
- Howarth, R.; Chan, F.; Conley, D. J.; Garnier, J.; Doney, S. C.; Marino, R.; Billen, G.: Coupled biogeochemical cycles. Eutrophication and hypoxia in temperate estuaries and coastal marine ecosystems. In: *Frontiers in Ecology and the Environment*, 9, 1, 18–26, 2011.
- IKSE: Die Elbe und ihr Einzugsgebiet. Ein geographisch-hydrologischer und wasserwirtschaftlicher Überblick. In German, International Commission for the Protection of the Elbe, Magdeburg, 2005.
- Kärnä, T.; Baptista, A. M.: Water age in the Columbia River estuary. In: *Estuarine, Coastal and Shelf Science*, 183, 249–259, 2016.
- Kemp, W. M.; Boynton, W. R.: Influence of biological and physical processes on dissolved oxygen dynamics in an estuarine system. Implications for measurement of community metabolism. In: *Estuarine and Coastal Marine Science*, 11, 4, 407–431, 1980.
- Kemp, W. M.; Testa, J. M.; Conley, D. J.; Gilbert, D.; Hagy, J. D.: Temporal responses of coastal hypoxia to nutrient loading and physical controls. In: *Biogeosciences*, 6, 12, 2985–3008, 2009.
- Lane, A.: Bathymetric evolution of the Mersey Estuary, UK, 1906–1997. Causes and effects. In: *Estuarine, Coastal and Shelf Science*, 59, 2, 249–263, 2004.
- Lanoux, A.; Etcheber, H.; Schmidt, S.; Sottolichio, A.; Chabaud, G.; Richard, M.; Abril, G.: Factors contributing to hypoxia in a highly turbid, macrotidal estuary (the Gironde, France). In: *Environmental Science: Processes & Impacts*, 15, 3, 585, 2013.
- Liu, W.-C.; Hsu, M.-H.; Kuo, A. Y.; Li, M.-H.: Influence of bathymetric changes on hydrodynamics and salt intrusion in estuarine system. In: *Journal of the American Water Resources Association*, 37, 5, 1405–1416, 2001.
- Luketina, D.: Simple Tidal Prism Models Revisited. In: *Estuarine, Coastal and Shelf Science*, 46, 1, 77–84, 1998.
- Meire, P.; Ysebaert, T.; van Damme, S.; van den Bergh, E.; Maris, T.; Struyf, E.: The Scheldt estuary. A description of a changing ecosystem. In: *Hydrobiologia*, 540, 1–3, 1–11, 2005.
- Meyers, S. D.; Linville, A. J.; Luther, M. E.: Alteration of residual circulation due to large-scale infrastructure in a coastal plain estuary. In: *Estuaries and Coasts*, 37, 2, 493–507, 2014.

- Middelburg, J. J.; Herman, P. M. J.: Organic matter processing in tidal estuaries. In: *Marine Chemistry*, 106, 1–2, 127–147, 2007.
- Monsen, N. E.; Cloern, J. E.; Lucas, L. V.; Monismith, S. G.: A comment on the use of flushing time, residence time, and age as transport time scales. In: *Limnology and Oceanography*, 47, 5, 1545–1553, 2002.
- Paerl, H. W.: Assessing and managing nutrient-enhanced eutrophication in estuarine and coastal waters. Interactive effects of human and climatic perturbations. In: *Ecological Engineering*, 26, 1, 40–54, 2006.
- Paerl, H. W.: Controlling eutrophication along the freshwater–marine continuum. Dual nutrient (N and P) reductions are essential. In: *Estuaries and Coasts*, 32, 4, 593–601, 2009.
- Picado, A.; Dias, J. M.; Fortunato, A. B.: Tidal changes in estuarine systems induced by local geomorphologic modifications. In: *Continental Shelf Research*, 30, 17, 1854–1864, 2010.
- Postma, L.; Boderie, P. M. A.; van Gils, J. A. G.; van Beek, J. K. L.: Component software systems for surface water simulation. In: Goos, G.; Hartmanis, J.; van Leeuwen, J.; Sloot, P. M. A.; Abramson, D.; Bogdanov, A. V.; Dongarra, J. J.; Zomaya, A. Y.; Gorbachev, Y. E. (eds.): *Computational Science — ICCS 2003*, Springer Berlin Heidelberg, Berlin, Heidelberg, 649–658, doi: 10.1007/3-540-44860-8_67, 2003.
- Prandle, D.: Relationships between tidal dynamics and bathymetry in strongly convergent estuaries. In: *Journal of Physical Oceanography*, 33, 12, 2738–2750, 2003.
- Rabalais, N. N.; Díaz, R. J.; Levin, L. A.; Turner, R. E.; Gilbert, D.; Zhang, J.: Dynamics and distribution of natural and human-caused hypoxia. In: *Biogeosciences*, 7, 2, 585–619, 2010.
- Rayson, M. D.; Gross, E. S.; Hetland, R. D.; Fringer, O. B.: Time scales in Galveston Bay. An unsteady estuary. In: *Journal of Geophysical Research: Oceans*, 121, 4, 2268–2285, 2016.
- Ren, Y.; Lin, B.; Sun, J.; Pan, S.: Predicting water age distribution in the Pearl River Estuary using a three-dimensional model. In: *Journal of Marine Systems*, 139, 276–287, 2014.
- Ruiz, J.; Polo, M. J.; Díez-Minguito, M.; Navarro, G.; Morris, E. P.; Huertas, E.; Caballero, I.; Contreras, E.; Losada, M. A.: The Guadalquivir Estuary. A hot spot for environmental and human conflicts. In: Finkl, C. W.; Makowski, C. (eds.): *Environmental Management and Governance. Advances in Coastal and Marine Resources*, Springer International Publishing, Cham, 199–232, doi: 10.1007/978-3-319-06305-8_8, 2015.
- Savenije, H. H. G.: *Salinity and tides in alluvial estuaries* Elsevier, Amsterdam, 2005.
- Schöl, A.; Hein, B.; Wyrwa, J.; Kirchesch, V.: Modelling Water Quality in the Elbe and its Estuary. Large scale and long term applications with focus on the oxygen budget of the estuary. In: *Die Küste*, 81, 203–232, 2014.
- Schroeder, F.: Water quality in the Elbe estuary: Significance of different processes for the oxygen deficit at Hamburg. In: *Environmental Modeling and Assessment*, 73–82, 1997.
- Scully, M. E.: Physical controls on hypoxia in Chesapeake Bay. A numerical modeling study. In: *Journal of Geophysical Research: Oceans*, 118, 3, 1239–1256, 2013.

Sehili, A.; Lang, G.; Lippert, C.: High-resolution subgrid models: background, grid generation, and implementation. In: *Ocean Dynamics*, 2014.

Sharp, J. H.: Estuarine oxygen dynamics. What can we learn about hypoxia from long-time records in the Delaware Estuary? In: *Limnology and Oceanography*, 55, 2, 535–548, 2010.

Sheldon, J. E.; Alber, M.: The calculation of estuarine turnover times using freshwater fraction and tidal prism models. A critical evaluation. In: *Estuaries and Coasts*, 29, 1, 133–146, 2006.

Shen, J.; Haas, L.: Calculating age and residence time in the tidal York River using three-dimensional model experiments. In: *Estuarine, Coastal and Shelf Science*, 61, 3, 449–461, 2004.

Shen, J.; Lin, J.: Modeling study of the influences of tide and stratification on age of water in the tidal James River. In: *Estuarine, Coastal and Shelf Science*, 68, 1–2, 101–112, 2006.

Smits, J. G. C.; van Beek, J. K. L.: ECO: a generic eutrophication model including comprehensive sediment-water interaction. In: *PLoS ONE*, 8, 7, e68104, 2013.

Tomaso, D. J.; Najjar, R. G.: Long-term variations in the dissolved oxygen budget of an urbanized tidal river. The upper Delaware Estuary. In: *Journal of Geophysical Research: Biogeosciences*, 120, 6, 1027–1045, 2015.

van Damme, S.; Struyf, E.; Maris, T.; Ysebaert, T.; Dehairs, F.; Tackx, M.; Heip, C.; Meire, P.: Spatial and temporal patterns of water quality along the estuarine salinity gradient of the Scheldt estuary (Belgium and The Netherlands). Results of an integrated monitoring approach. In: *Hydrobiologia*, 540, 1–3, 29–45, 2005.

van Maren, D. S.; van Kessel, T.; Cronin, K.; Sittoni, L.: The impact of channel deepening and dredging on estuarine sediment concentration. In: *Continental Shelf Research*, 95, 1–14, 2015.

Verity, P. G.; Alber, M.; Bricker, S. B.: Development of hypoxia in well-mixed subtropical estuaries in the Southeastern USA. In: *Estuaries and Coasts*, 29, 4, 665–673, 2006.

Vriend, H. J. de; Wang, Z. B.; Ysebaert, T.; Herman, P. M. J.; Ding, P.: Eco-Morphological Problems in the Yangtze Estuary and the Western Scheldt. In: *Wetlands*, 31, 6, 1033–1042, 2011.

Walther, R.; Cayrol, C.; Hamm, L.; Delouis, A.; Leahy, D.: Evaluation of an offshore disposal site in the Loire Estuary through field monitoring and 3D numerical modeling. In: *Coastal Engineering Proceedings*, 1, 34, 24, 2015.

Zhang, H.; Li, S.: Effects of physical and biochemical processes on the dissolved oxygen budget for the Pearl River Estuary during summer. In: *Journal of Marine Systems*, 79, 1–2, 65–88, 2010.

Zimmerman, J. T. F.: Estuarine residence times. In: Kjerfve, B. (ed.): *Hydrodynamics of estuaries*, CRC Press, Boca Raton, 75–84, 1988.